Paper No.
9160

NACE INTERNATIONAL CORROSION 2017 Conference & Expo

Effect of Solution pH on Corrosion Product Layer Formation in a Controlled Water Chemistry System

Supat Ieamsupapong,[1] Bruce Brown, Marc Singer, and Srdjan Nesic
Institute for Corrosion and Multiphase Technology
Department of Chemical & Biomolecular Engineering, Ohio University
342 West State Street, Athens, OH 45701 U.S.A.

ABSTRACT

The primary objective of this study was to investigate iron carbonate ($FeCO_3$) formation mechanisms on ferritic-pearlitic carbon steel corroding in a CO_2 saturated aqueous solution near iron carbonate saturation, with particular emphasis on the effect of solution pH. A controlled water chemistry test apparatus was developed to resolve issues with drifting water chemistry during long-term corrosion experiments. An improved test apparatus for holding the metal samples was also introduced to eliminate the non-uniformity of flow across the samples and assure well controlled mass transfer conditions in the glass cell. Results pertaining to the solution pH effect are presented by discussing associated water chemistry, corrosion rates, and $FeCO_3$ morphologies. Under the controlled water chemistry conditions, iron carbide (Fe_3C) was found to play a critical role in the formation of $FeCO_3$ near the steel surface, where ferrous ions accumulate and surface pH is higher than solution pH. Experiments within the pH range (pH 5.4-6.0) resulted in similar corrosion product characteristics and corrosion rates given that the level of $FeCO_3$ saturation was controlled. It was found that a higher solution pH was likely to give a slightly better protection to the steel surface.

Key words: Solution pH; Controlled water chemistry; $FeCO_3$; Carbon steel

INTRODUCTION

It has been verified both experimentally and computationally that pH has a strong effect on aqueous CO_2 corrosion of carbon steel.[1] At a high pH value, the solubility of $FeCO_3$ decreases and results in a higher precipitation rate.[2,3] Solution pH is calculated directly from the hydrogen ion concentration that results

[1] Currently with Department of Production Engineering, Faculty of Engineering, King Mongkut's University of Technology North Bangkok, 1518 Pracharat I Rd., Wongsawang, Bangsue, Bangkok 10800 Thailand

from the dissociation of the carbonate and bicarbonate in aqueous solution.[7] Furthermore, bicarbonate dissociation leads to the generation of carbonate ion. Hence, the pH i.e. the concentration of hydrogen ions is linked to the concentration of carbonate ion, which is an important parameter for determining the saturation value ($S_{[FeCO3]}$) as expressed in Equation (1).

$$S_{[FeCO3]} = \frac{[Fe^{2+}][CO_3^{2-}]}{K_{sp}} \quad (1)$$

Many methods have been proposed to measure surface pH directly[4,5] and indirectly[6,7,8]. It is understood that a reduction in the general CO_2 corrosion rate of mild steel occurs at higher pH when the solubility of $FeCO_3$ decreases. Figure 1 shows the solution pH effect on solubility of $FeCO_3$. The $S_{[FeCO3]}$ = 1 line represents saturation with respect to $FeCO_3$ while the dashed lines represent a factor of two from the saturation value. The region on the right of the saturation value represents a supersaturated solution with respect to $FeCO_3$, where protective $FeCO_3$ layers form and corrosion rates are uniformly low. The region on the left represents an undersaturated solution with respect to $FeCO_3$, where protective $FeCO_3$ layers are not going to form, and uniform "bare steel" corrosion is a result. Both of these regions have been explored experimentally in the past. However the intermediate conditions is where limited information on CO_2 corrosion is available and the corrosion behavior seems to be sensitive to small variations in environmental conditions, in some cases resulting in localized attack.[9] In order to address this issue, more in-depth research on corrosion mechanisms and $FeCO_3$ formation in the midrange of solution pH 5.4-6.0 is needed.

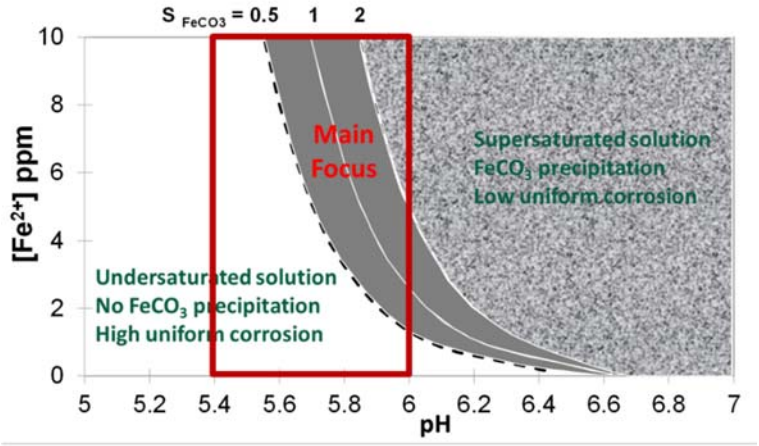

Figure 1: The solution pH effect on solubility of $FeCO_3$ generated for 80°C and pCO_2 of 0.53 bar.

EXPERIMENTAL PROCEDURE

Experimental Setup

In order to better simulate conditions from the field and maintain a stable water chemistry in long-term lab experiments, a system with continuous replenishment of the solution was used. This system consists of multiple CO_2-purged glass cells with controlled water chemistry. The first two are conditioning cells in the system that feed the electrolyte into a 2-liter working cell and flush out the excess amount of corrosion products (ferrous ions) generated by the actively corroding samples in long-term experiments. The aim of this flow-through system is to have the ability to maintain a stable water chemistry during long corrosion experiments; a secondary benefit is a minimization of reagent use and waste generation. Figure 2 shows

the flow-through system that consists of multiple feed solution containers and the working cell. There we can see an impeller system complemented with specialized specimen holders designed to maintain uniform flow and mass transfer in the cell. The concentrations of species in the feed solution is calculated and adjusted based on the desired working conditions in the working cell to ensure that water chemistry can be maintained throughout the entire duration of the experiments. Figure 3 shows the top view of the sample holder design in a 2-liter working cell. All samples are located at the same height and same radial distance from the impeller in order to give similar mass transfer rates. Figure 4 shows limiting currents that were used to define the mass transfer coefficient of this system by using ferri-ferrocyanide coupled reactions for this particular flow-through setup.

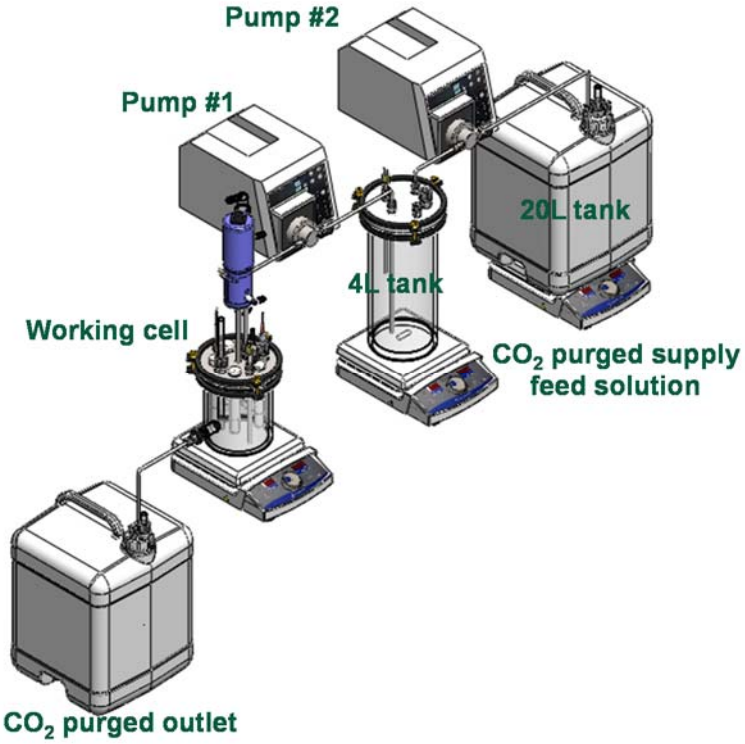

Figure 2: Flow-through setup to control solution pH and [Fe^{2+}]

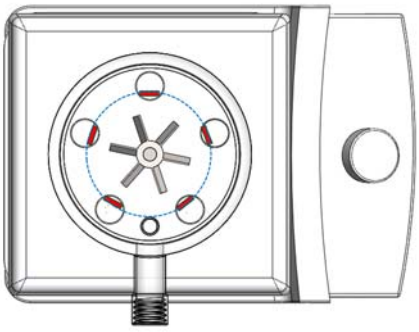

Figure 3: Top view of new sample holder design that gives well-controlled and uniform flow to all samples

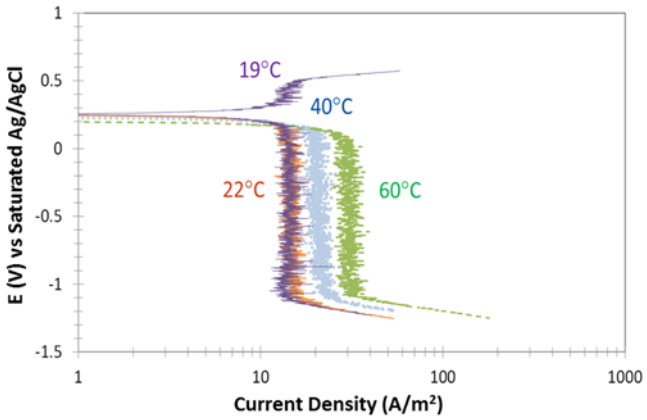

Figure 4: Mass transfer coefficient determination using ferri-ferrocyanide coupled reactions for the impeller and specialized sample holder setup

Sample preparation

The working cell, 4-liter feed tank and the 20-liter holding tank were filled with 1 wt.% NaCl aqueous electrolyte. The electrolyte in the 20-liter tank was kept at room temperature (30°C) while the 4-liter and 20-liter tank were heated to the desired temperature. The electrolyte in each tank was deaerated by continuously sparging with CO_2 at least for 2 hours before the pH adjustment. Subsequently, the solution pH was adjusted by addition of deaerated 1 M $NaHCO_3$. An equilibrium water chemistry model was used to calculate the desired concentrations of aqueous species such as Fe^{2+}, H^+, HCO_3^-, CO_3^{2-} which were maintained throughout the duration of the experiments. The heaters were used to control the temperature of electrolyte in the two tanks during the experiment.

Four UNS G10180 steel specimens with dimension of 12.6 mm x 12.6 mm x 2.5 mm were polished sequentially with 150, 400, and 600 grit sand paper, ultrasonicated in isopropanol, and air dried. After sample preparation, the sample holders in the working cell were lifted out of electrolyte for sample insertion into the specialized sample holder's slots, clamped in place, and immersed in the electrolyte.

After starting the experiment, ferrous ion concentration in the working cell was measured periodically (once or twice a day) by UV/Vis spectrophotometry (Thermo Scientific GENESIS 10 Vis). The solution pH in all tanks were continuously monitored and recorded when ferrous ion concentration measurements were performed. The measured ferrous ion concentration and solution pH values were used to determine the amount of fluid flow needed from the 4-liter feed tank. The flow rate (ranging from 2-20 ml/min) was provided by two pumps. The electrolyte level in the working cell and the 4-liter tank was controlled by mechanical floating switches.

Table 1 shows details of experimental parameters used to study the effect of solution pH on $FeCO_3$ formation near saturation conditions, conducted with the flow-through system described above. All of the test parameters were kept the same at 80°C, pCO_2 of 0.53 bar, 1 wt.% NaCl, and flow velocity of 0.6 m/s while maintaining the $FeCO_3$ saturation value close to unity in all test conditions; the only exception was the solution pH. Different ferrous ion concentration in each test were used to maintain the same $FeCO_3$ saturation value at different solution pH values. Also, UNS G10180 steel, which has a ferritic-pearlitic microstructure, was used. The microstructure of the test steel (UNS G10180) is shown in Figure 5.

Table 1
List of parameters for investigating effect of solution pH on $FeCO_3$ formation in controlled water chemistry conditions

Parameters	Test 1	Test 2	Test 3
Investigate	**Solution pH**		
Material	UNS G10180 (Ferrite-pearlite)		
Surface analysis techniques	SEM/EDS, XRD		
Electrochemical techniques	OCP, LPR		
Temperature	80°C		
Partial pressure of CO_2	0.53 bar		
Solution pH	**5.4**	**5.7**	**6.0**
$[Fe^{2+}]$	**40 ppm**	**10 ppm**	**3 ppm**
Target bulk $S_{[FeCO3]}$	**1**		
Electrolyte	1 wt% NaCl		
Method for inducing precipitation	Corrosion-driven		
Flow velocity	0.6 m/s		

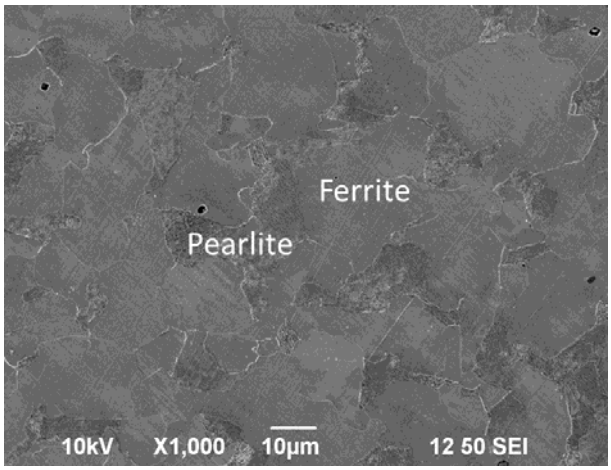

Figure 5: The microstructure of UNS G10180 along with its metallographic phases

Electrochemical measurements

In addition to the four weight loss specimen, a special specimen was made from the same steel stock and used for electrochemical measurements. This specimen was partially embedded in an epoxy, with 1.6 cm^2 exposed surface area. The working cell contained a conventional three-electrode electrochemical setup configuration (with Ag/AgCl as a reference electrode, Pt as a counter electrode, and carbon steel specimen as a working electrode). A potentiostat was used to measure linear polarization resistance (LPR). The working electrode was polarized from -5 mV to +5 mV with respect to the open circuit potential (OCP) at a scan rate of 0.125 mV/s. The LPR measurements were carried out every two hours in all experiments. The current density (i_{corr}) was calculated from the measured polarization resistance (Rp) according to the Stern-Geary equation.[10] In this work, the "B" constant of 26 mV was used.

RESULTS AND DISCUSSION

Water Chemistry

Figure 6 shows the comparison of ferrous ions change over the entire testing time for the experiments conducted at pH 5.4, 5.7, and 6.0. The target ferrous ions for the test conducted at pH 5.4, 5.7, and 6.0 were 40, 10, and 3 ppm, respectively. Figure 7 shows the comparison of solution pH change over time for the test conducted at pH 5.4, 5.7, and 6.0. Solution pH in all tests was maintained around the target pH value for the entire test, within 0.1 pH unit. Figure 8 shows the comparison of saturation value with respect to $FeCO_3$ for the test conducted at pH 5.4, 5.7, and 6.0. The iron carbonate saturation values of all the tests were maintained within a factor of two around the saturation level of one.

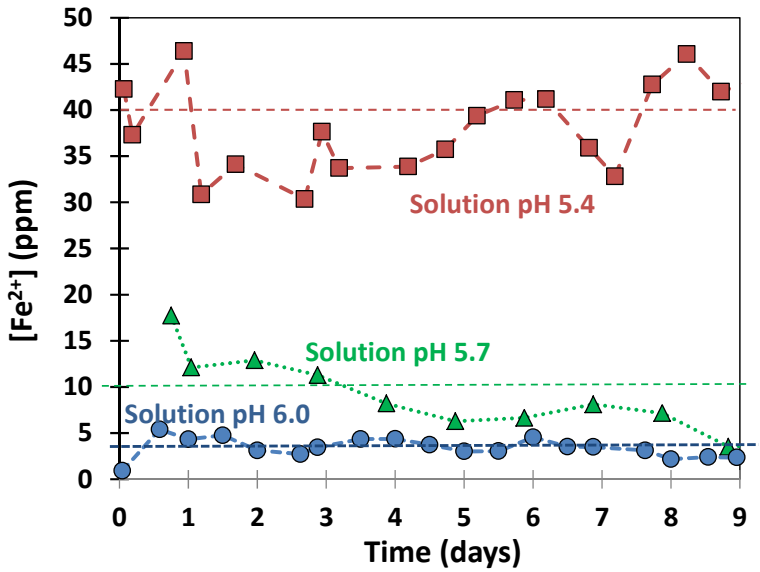

Figure 6: Comparison of $[Fe^{2+}]$ change over time using corrosion-driven precipitation method for the test conducted on UNS G10180 with solution pH range of 5.4-6.0 under conditions: T=80^{0}C, pCO_2 = 0.53 bar, 0.6 m/s

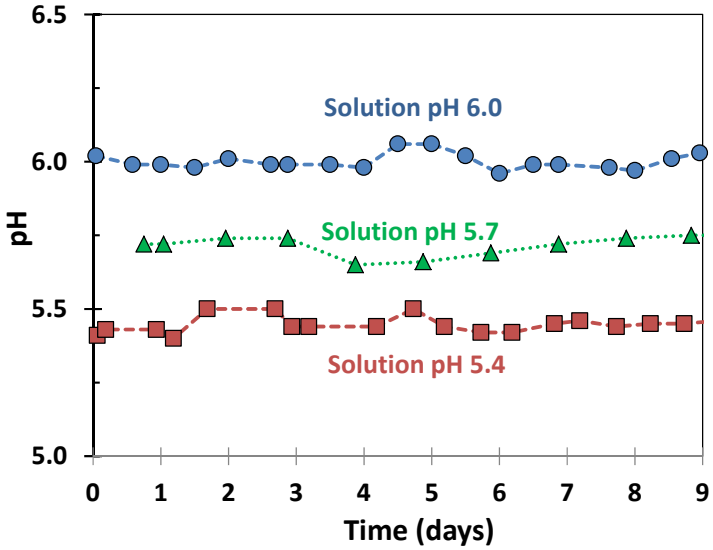

Figure 7: Comparison of pH change over time using corrosion-driven precipitation method for the test conducted on UNS G10180 with solution pH range of 5.4-6.0 under conditions: T=80^{0}C, pCO_2 = 0.53 bar, 0.6 m/s

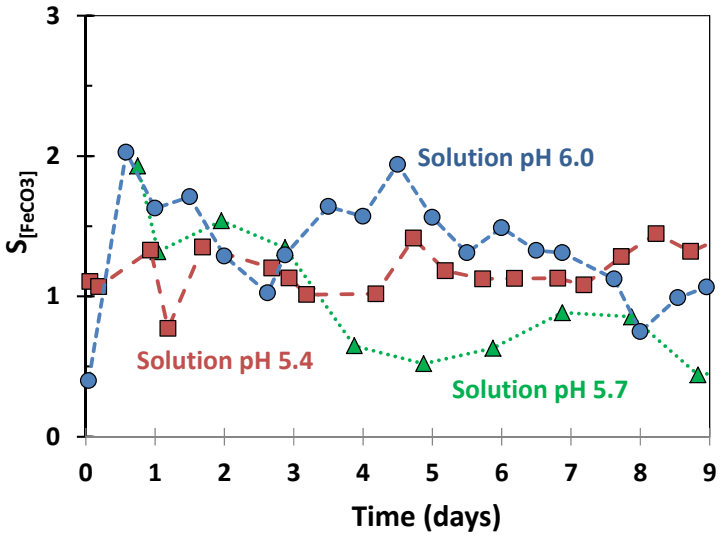

Figure 8: Comparison of $S_{[FeCO3]}$ change over time using corrosion-driven precipitation method for the test conducted on UNS G10180 with solution pH range of 5.4-6.0 under conditions: T=80^{0}C, pCO_2 = 0.53 bar, 0.6 m/s

Corrosion rates

Figure 9 shows the comparison of corrosion rate behavior over time for the test conducted on UNS G10180 with solution pH 5.4, 5.7, and 6.0 under conditions: T=80^{0}C, pCO_2 = 0.53 bar, 0.6 m/s. Slightly higher beginning and ending corrosion rates for the lower pH values were observed as expected from theory. The steady increase in corrosion rates at the beginning, during the “active corrosion” region, for the experiments with UNS G10180 materials was caused by the effect of iron carbide that was left behind when the ferrite dissolved from actively corroding steel surface. In general, the corrosion rate behavior of tests in pH range of 5.4-6.0 was similar. The higher pH value seemed to give only a slightly better

protection to the steel surface for the same saturation level of $FeCO_3$. Figure 10 shows the comparison between the open circuit potential over time for the test conducted on UNS G10180 for each solution pH of 5.4, 5.7, and 6.0. The open circuit potential increase for solution pH 5.4 and pH 6.0 has two main stages: the first one is due to the iron carbide buildup that is left behind from corrosion and the second is due to formation of $FeCO_3$ and pseudo-passivation of the steel surface.

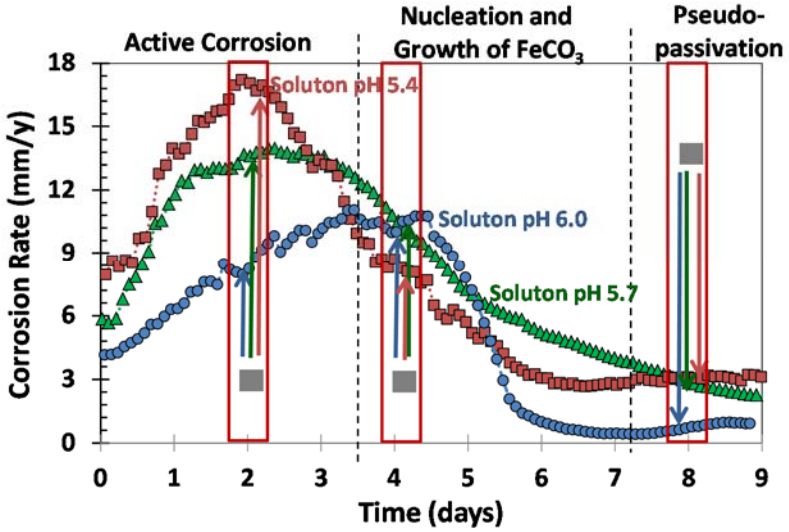

Figure 9: Comparison of corrosion rate behavior over time using corrosion-driven precipitation method for the test conducted on UNS G10180 with solution pH range of 5.4-6.0 under conditions: T=80^{0}C, pCO_2 = 0.53 bar, 0.6 m/s

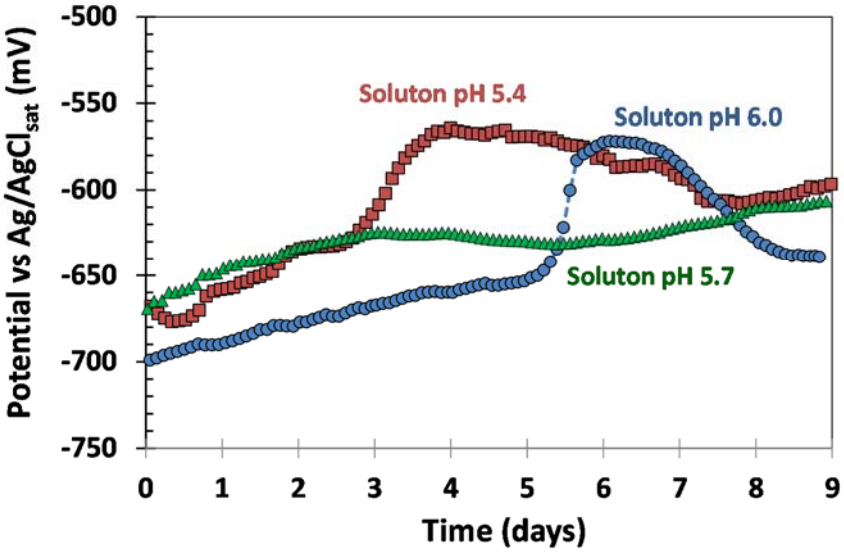

Figure 10: Comparison of open circuit potential over time using corrosion-driven precipitation method for the test conducted on UNS G10180 with solution pH range of 5.4-6.0 under conditions: T=80^{0}C, pCO_2 = 0.53 bar, 0.6 m/s

Corrosion Morphologies

Surface morphology

Scanning electron microscopy (SEM) was used to analyse the surface and cross-section morphologies. X-ray diffraction (XRD) was used to identify phases of the corrosion products. Figure 11 shows the comparison of surface morphologies of corrosion products on UNS G10180 conducted with solution pH range of 5.4 to 6.0. It can be seen that surface morphology of all UNS G10180 samples are similar regardless of the bulk solution pH value or the time that the samples were extracted from the experiment.

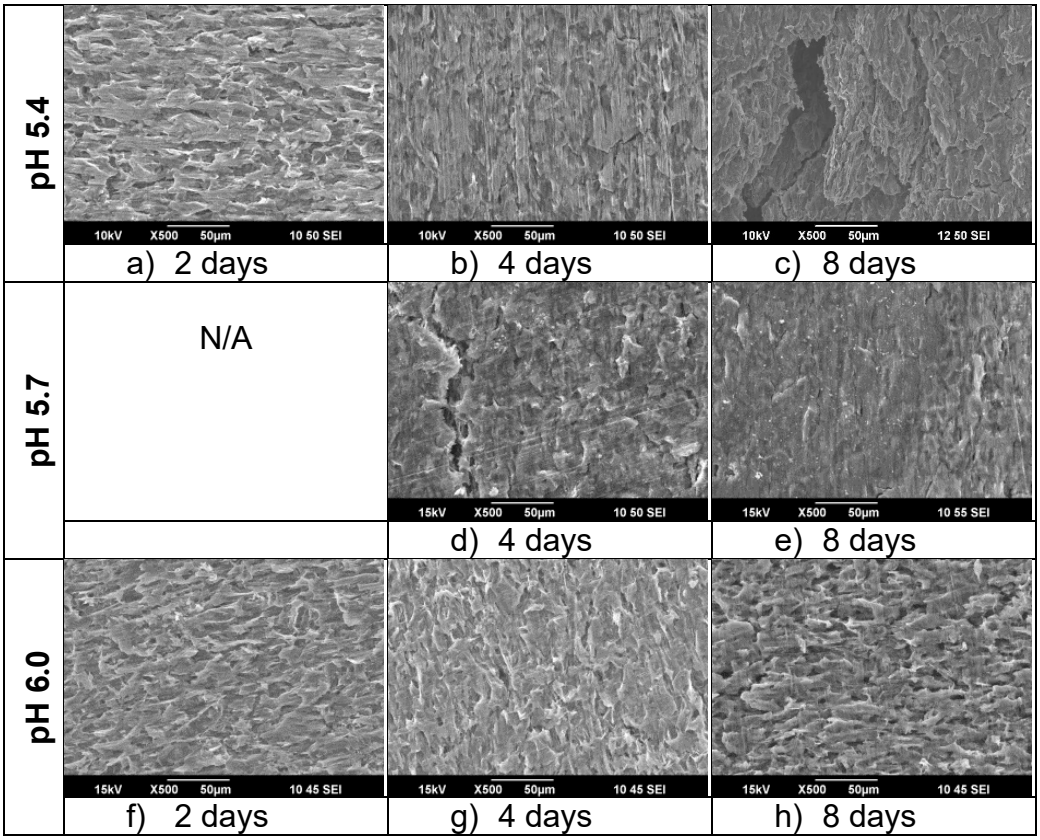

Figure 11: Comparison of surface morphologies of samples from the test conducted on UNS G10180 with solution pH range of 5.4-6.0 under conditions: T=80^{0}C, pCO_2 = 0.53 bar, and 0.6 m/s

X-ray diffraction (XRD)

In addition to visual observations, X-ray diffraction was used to identify the phase of corrosion products on sample surface extracted from the experiments conducted with UNS G10180. Figure 12 shows the comparison of phases identified by XRD on the sample that were exposed for 4 and 8 days. The Fe_3C and Fe peaks were detected on samples extracted from the initial periods of corrosion. The $FeCO_3$ was an additional phase detected on the sample extracted from the subsequent pseudo-passivation period.

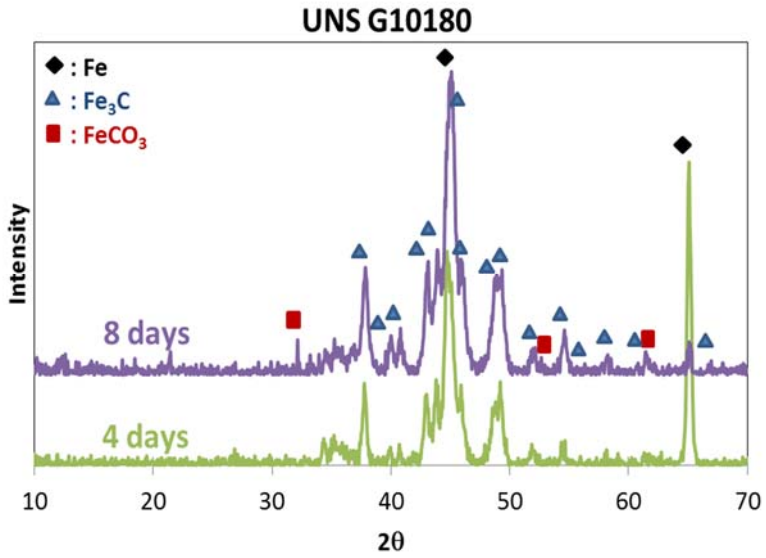

Figure 12: XRD pattern on samples from the tests conducted with UNS G 10180 at 80°C, pCO_2 = 0.53 bar, solution pH 5.7, flow velocity of 0.6 m/s.

Cross-section morphology

Figure 13 shows the comparison of cross-section morphologies of corrosion products from the specimens extracted at different time intervals from the experiments conducted on UNS G10180 with solution pH in a range of 5.4-6.0. The observation of these cross-section morphologies was consistent with other findings for each of the surface morphologies. The cross-section morphology gives more useful details regarding the corrosion product layer formed. Each row shows the evolution of corrosion product layers developed on UNS G10180 mild steel samples for a given solution pH value. Figure 13a) and Figure 13g) depict the beginning of corrosion product developed during early stage of corrosion or 'active corrosion' period as defined in corrosion rates vs. time curve. Figure 13b), Figure 13d), and Figure 13h) capture the beginning of the formation of iron carbonate within the iron carbide matrix in the 'nucleation and growth of $FeCO_3$' period. Figure 13c), Figure 13f), and Figure 13i) show iron carbonate was formed mostly near the steel surface and helped to slow down the corrosion rate in the 'pseudo-passivation' period. Although the presence of iron carbonate significantly reduced corrosion rates from the initial rate, the final corrosion rates observed were still relatively high. This agrees with the corrosion rate measured by LPR as shown in Figure 9.

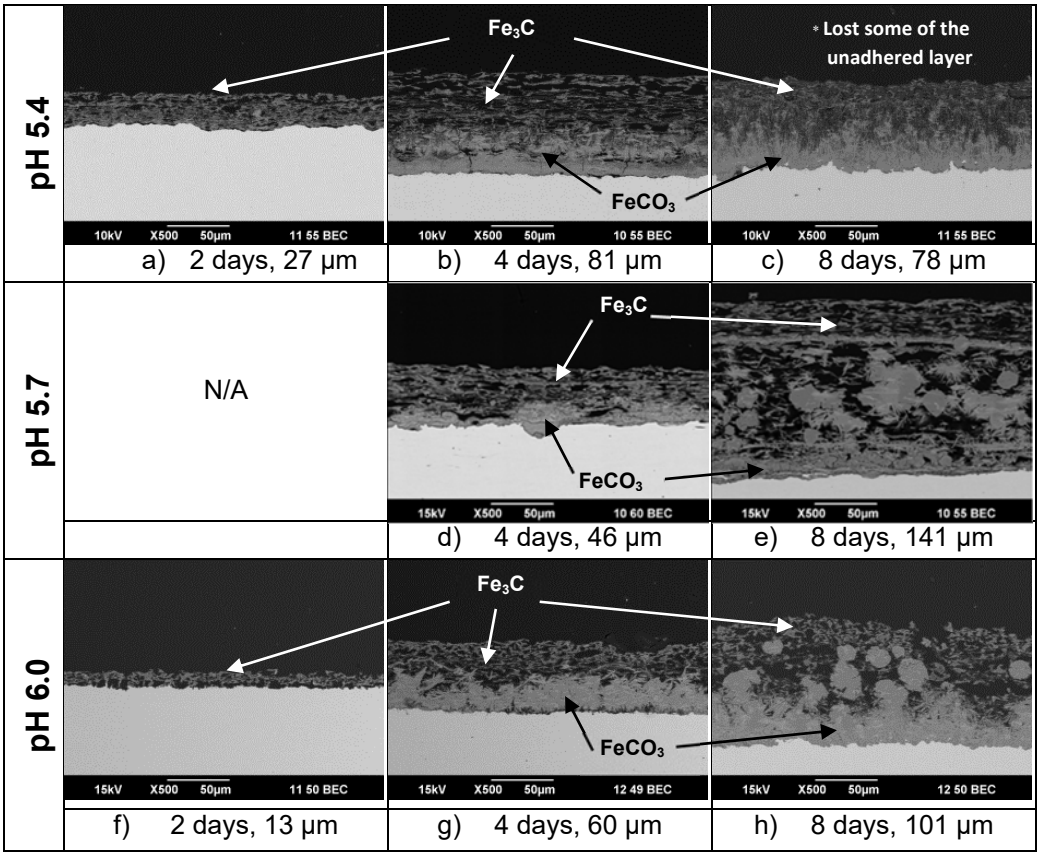

Figure 13: Comparison of cross-section morphologies of samples from the test on UNS G10180 with solution pH range of 5.4-6.0 under conditions: T=80^{0}C, pCO_2 = 0.53 bar, initial solution pH 5.7, 0.6 m/s

Protection conferred by corrosion product layers

The well-adhering corrosion product layers formed at the end of these experiments, (see Figure 13), can give a degree protection to the UNS G10180 steel substrate from further corrosion. However, the undermining by the corrosion process occurring between the iron carbonate layer and steel interface can be clearly observed by the small dark areas between the light colored steel at the bottom of the image and the gray colored areas of the corrosion product layer in the cross-section morphologies, as shown in Figure 14a-c). This undermining lead to a relatively high final corrosion rate (always greater than 1 mm/yr) measured by LPR after 8-9 days, shown in Table 2. The level of protectiveness by the iron carbonate layer was not as high in these experiments, possibly because the bulk solution water chemistry in these tests was controlled near the $FeCO_3$ saturation value. Thus, the level of protectiveness would be expected to improve if a higher level of $FeCO_3$ saturation in the bulk solution was used.

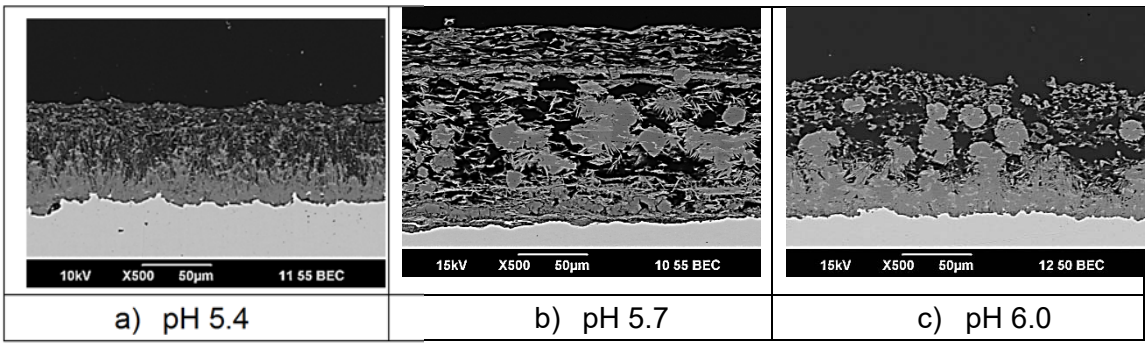

Figure 14: Undermining effect observed on cross-section morphologies of UNS G10180 samples with solution pH range of 5.4-6.0 for 8-9 days

Table 2
Comparison of ending corrosion rates around 8-9 days of the tests conducted on UNS G10180 with solution pH 5.4-6.0 at 80°C, pCO_2 = 0.53 bar, and flow velocity of 0.6 m/s

	Corrosion Rate for 8-9 days
pH 5.4	~3 mm/y
pH 5.7	~2 mm/y
pH 6.0	~1 mm/y

CONCLUSIONS

For the range of solution pH investigated in this study, it was found that:

- Under controlled water chemistry conditions, evidences suggested that Fe_3C played a critical role in the formation of $FeCO_3$ near the steel surface, where Fe^{2+} accumulate and surface pH is higher than bulk solution pH.
- When bulk saturation of $FeCO_3$ is controlled, similar corrosion product layers and corrosion rates were observed over the pH range of 5.4-6.0.
- When bulk saturation of $FeCO_3$ was maintained around one, only partially protective layers formed, irrespective of pH.

ACKNOWLEDGEMENTS

The authors greatly appreciate: Dr. Bert Pots for fruitful discussion on water chemistry control, Cody Shafer for providing the technical help and images of the test apparatus in this research, and Dr. Fernando Farelas for the help on etched microstructure. The authors also would like to acknowledge the industrial sponsors who have supported the Corrosion Center JIP over the period of this research (Anad0arko, Baker Hughes, BP, Chevron, China National Offshore Oil Corporation, ConocoPhillips, DNV GL, ExxonMobil, M-I SWACO, Occidental Oil Company, Petroleum Institute, PTT, Saudi Aramco, Shell Global Solutions, SINOPEC, TOTAL, TransCanada, WGK.)

REFERENCES

1. S. Nesic, "Key issues related to modelling of internal corrosion of oil and gas pipelines – A review," *Corrosion Science,* vol. 49, pp. 4308-4338, 2007.
2. K. Chokshi, W. Sun, and S. Nesic, "Iron carbonate scale growth and the effect of inhibition in CO_2 corrosion of mild steel " in *CORROSION/2005, Paper No. 05285, (Houston, TX: NACE, 2005)*.
3. M. H. Nazari, S. R. Allahkaram, and M. B. Kermani, "The effects of temperature and pH on the characteristics of corrosion product in CO_2 corrosion of grade X70 steel," *Materials and Design,* vol. 31, pp. 3559-3563, 2010.
4. F. King, C. D. Litke, and Y. Tang, "Effect of interfacial pH on the reduction of oxygen on copper in neutral $NaClO_4$ solution," *Journal of Electroanalytical Chemistry,* vol. 384, pp. 105−113, 1995.
5. T. Yoshinobu, T. Harada, and H. Iwasaki, "Application of pH-Imaging sensor to determining the diffusion coefficients of ions in electrolytic solutions," *Japanese Journal of Applied Physics,* vol. 39, pp. L318−L320, 2000.
6. Z. Lewandowski, W. C. Lee, W. G. Charazklis, and B. Little, "Dissolved oxygen and pH microelectrode measurements at water-immersed metal surfaces," *Corrosion,* vol. 45, pp. 92−98, 1989.
7. C. Deslouis, I. Frateur, G. Maurin, and B. Tribollet, "Interfacial pH measurement during the reduction of dissolved oxygen in a submerged impinging jet cell," *Journal of Applied Electrochemistry,* vol. 27, pp. 482-492, 1997.
8. T. Honda, K. Murase, T. Hirato, and Y. Awakura, "pH measurement in the vicinity of a cathode evolving hydrogen gas using an antimony microelectrode," *Journal of Applied Electrochemistry,* vol. 28, pp. 617−622, 1998.
9. Y. Sun and S. Nesic, "A parametric study and modeling on localized CO_2 corrosion in horizontal wet gas flow," in *CORROSION/2004, Paper No. 04380, (Houston, TX: NACE, 2004)*.
10. M. Stern and A. L. Geary, Electrochemical polarization I. A theoretical analysis of the shape of polarization curves, J. Electrochem. Soc. 104 (1957) 56.